Detection of HCl molecules by resonantly enhanced third-harmonic generation, driven by midinfrared laser pulses

Jan Frederic Kinder,* Fabian Cipura, and Thomas Halfmann
Institut für Angewandte Physik, Technische Universität Darmstadt, Hochschulstr. 6, 64289 Darmstadt, Germany

(Received 29 March 2021; accepted 7 May 2021; published 26 May 2021)

We studied resonantly enhanced third-harmonic generation, induced by midinfrared, spectrally narrow-band, nanosecond laser pulses tuned in the vicinity of rovibrational molecular resonances. As we drive the frequency conversion process simultaneously close to single-, two-, and three-photon resonances, we get strong resonance enhancements of the third-harmonic yield by several orders of magnitude. The experimental setup requires only a single midinfrared laser beamline; the signal wavelength is easily separable from the much longer driving laser wavelength. We performed extended, systematic studies on the third-harmonic yield, spectral line shape and linewidth with laser intensity, frequency, and pressure. We determined a detection limit of 10^{15} molecules/cm^3, which indicates the potential of the approach for realistic applications in trace gas detection.

DOI: 10.1103/PhysRevA.103.052808

I. INTRODUCTION

Nonlinear laser spectroscopy offers a variety of techniques for sensitive detection of molecular species, with a multitude of applications in trace gas analysis, combustion diagnostics, environmental sensing, and microscopy. Stimulated Raman scattering and coherent anti-Stokes Raman-scattering (CARS) are considered the workhorses for such purposes [1–3]. CARS relies on a resonantly enhanced four-wave mixing process, driven by a pump laser pulse at frequency ω_P and a Stokes laser pulse at frequency ω_S, typically with wavelengths in the visible or near-ultraviolet regime. The lasers are tuned to two-photon resonance with vibrational states in the electronic ground state of a molecular species, generating a signal pulse at frequency $2\omega_P - \omega_S$. The signal yield in CARS benefits from the large transition dipole moment between the electronic ground and electronic excited states, as well as two-photon resonance with vibrational states. However, the pump and Stokes lasers are usually very far detuned (typically in the range of many $1000-10000\,\mathrm{cm}^{-1}$, expressed in units of wave numbers) from the single-photon transition to the excited electronic state. As two photons from the pump laser are involved in the frequency conversion process of CARS, these large detunings appear twice as limiting factors in the third-order nonlinear polarization. Moreover, CARS typically requires two laser pulses. Thus, for applications in trace gas detection, it would be desirable to find an alternative nonlinear technique, which requires only a single driving laser beam and permits operation at small (or zero) detunings at *all* single- and multiphoton transitions, involved in the frequency conversion process.

Third-harmonic generation (THG) is the lowest-order frequency conversion process, which occurs in any medium of any type of symmetry. It requires only a single driving laser beam. Hence, it would be a straightforward choice for nonlinear spectroscopy and analytics. THG was first demonstrated using a Ruby laser by Maker and Terhune, and afterward extensively investigated in a broad variety of media [4]. It is a parametric process, i.e., no energy from the incident fundamental radiation is deposited in the sample. This makes THG very well suited to investigate sensitive samples (e.g., from biology), and it meanwhile evolved into a standard technique for laser-based, nonlinear microscopy [5]. The latter applications are typically based upon off-resonant THG with fixed-frequency lasers. Thus, the driving laser is very far detuned from resonances to electronic states (which are typically at vacuum-ultraviolet (VUV) wavelengths) or vibrational states (which are typically in the mid-infrared regime). Off-resonant THG does not give spectral selectivity, which is required to detect a molecular species. THG via resonances enhances the signal yield [6] and provides the required spectral selectivity.

Resonantly enhanced THG via an electronic transition yields a signal in the VUV, which suffers from strong absorption in the medium or any background gas and optics in the detection pathway. Thus, resonantly enhanced THG (e.g., applied in atomic gases to generate coherent VUV radiation [7,8]) has to be fully implemented in a vacuum setup—which is not feasible for most applications in molecular spectrometry.

Resonant THG at vibrational transitions would be a promising route toward trace molecule detection under realistic conditions. However, the nonlinear process requires sufficiently intense laser pulses with tunability in the midinfrared (i.e., in the regime of vibrational fingerprint spectra) and narrow spectral bandwidth to maintain spectral selectivity. Such laser systems only became available in the last decade, mostly in homemade experimental setups and with spectral bandwidth typically still quite far above the Fourier-transform limit [9]. Recently, Miyamoto *et al.* applied a narrow-band, midinfrared laser system for coherent two-photon excitation

*jan-frederic.kinder@physik.tu-darmstadt.de

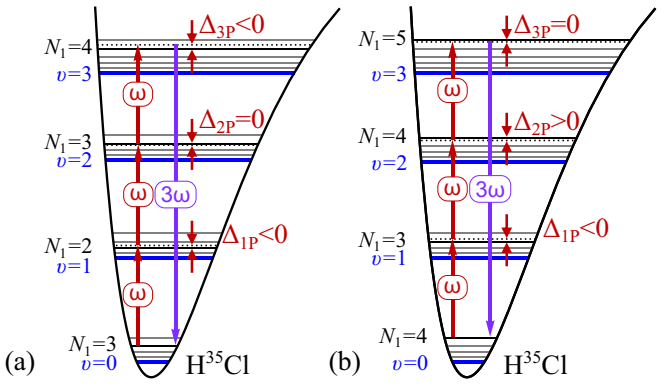

FIG. 1. Schematic level scheme for resonantly enhanced THG among rovibrational molecular states in the electronic ground state of HCl molecules. The states are labeled by vibrational quantum number ν and rotational quantum number N_1. Example (a) shows a two-photon resonance, example (b) a three-photon resonance.

and THG in hydrogen molecules [10]. However, the latter experiment was implemented in cryogenically cooled molecules at large pressures around 1 bar (thus, far beyond realistic conditions for trace detection), and THG was studied on a single resonance only. We note that also beyond THG, narrow-band and tunable laser sources in the midinfrared are a requisite for a wide range of proposed applications in nonlinear molecular spectroscopy [11].

We now turn our attention to resonance enhancements of THG in the regime of midinfrared vibrational transitions in a molecular species. Let us consider a ladder-type excitation scheme in the vicinity of the lowest vibrational states $\nu = 0, 1, 2, 3$ of a molecule (see Fig. 1). We get THG enhancement and spectral selectivity by tuning the driving laser either to the single-photon resonance between the ground state $\nu = 0$ and the first excited vibrational state $\nu = 1$, or to the two-photon resonance between states $\nu = 0$ and $\nu = 2$, or to the three-photon resonance between states $\nu = 0$ and $\nu = 3$. Due to the anharmonicity of the molecular potential, we can have the driving laser in resonance either at the single-, or two-, or three-photon transition, but never with several of them at the same time.

Tuning to the single-photon resonance would be a bad choice, as the driving fundamental laser beam is strongly absorbed on the single-photon resonance. Tuning the laser to the two-photon resonance would be a good choice. Neither the driving fundamental laser nor the THG signal would experience single-photon absorption in this case, as they are both tuned off such a resonance. The two-photon resonance enables an enhancement in the frequency conversion efficiency, similar to CARS. Tuning the driving laser to a three-photon resonance would also work well. Also, here the driving fundamental beam is off single-photon resonance and does not suffer from absorption. We note that we may expect reabsorption of the THG signal at the (single-photon) overtone transition between states $\nu = 3$ and $\nu = 0$. However, overtone transitions moments in small molecules are typically orders of magnitude weaker compared to transitions with $\Delta\nu = 1$. Hence, reabsorption of the THG signal at infrared wavelengths will be small in most cases—though it has to be considered in general. In summary, we expect THG resonance enhancements, when the fundamental laser is tuned to two-photon or three-photon resonance between the vibrational states $\nu = 0, 1, 2, 3$.

We would like to stress an important feature of the THG process via vibrational states. Let us consider the case of the laser tuned to two-photon resonance. As the anharmonicity of the molecular potential is small, also in the case of the two-photon resonance the driving laser is simultaneously very close to the single- and three-photon resonance (typically detuned only by $10-100\,\mathrm{cm}^{-1}$, expressed in units of wave numbers). Thus, all three detunings relevant for the nonlinear polarization are small. The THG conversion efficiency will be enhanced not only by the two-photon resonance but also benefits from the near-resonance conditions at the single- and three-photon transition. Similar arguments also hold true for the laser tuned to three-photon resonance between the vibrational states. This feature is a specific difference to CARS, where only the two-photon detuning is small (zero), while single- and three-photon detunings are very large. We note that the electronic transition moment exploited by CARS is typically an order of magnitude larger compared to the transition moment between vibrational states. However, the much smaller detunings in THG via vibrational resonances also compensate for the smaller transition moments. Recently, Traverso *et al.* applied a related approach to enhance the nonlinear susceptibility of Raman scattering via a two-photon vibrational resonance in methane molecules [12]. However, the latter required two laser pulses at different wavelengths and was implemented with broadband picosecond pulses, which do not provide spectral resolution to resolve rotational transitions, e.g., to determine the temperature of the sample.

The following paper deals with experimental studies on THG spectroscopy of molecular species, resonantly enhanced by tuning the driving laser to multiphoton resonances between vibrational states. This gives large THG enhancement and spectral selectivity. We apply midinfrared laser pulses, generated from a homemade, pulsed amplifier system for the continuous wave output of a commercial optical parametric oscillator (OPO). The amplified laser system provides tunable nanosecond laser pulses in the midinfrared with pulse energy in the mJ regime and narrow spectral bandwidth close to the Fourier transform limit.

II. BASICS OF RESONANTLY ENHANCED FREQUENCY CONVERSION

The efficiency of THG in a nonlinear medium is determined by the third-order susceptibility $\chi^{(3)}$, which depends upon the level structure in the nonlinear medium and the detuning of the driving laser from all possible three-photon pathways between the ground and excited states [13–15]. We consider now a ladder-type level scheme, e.g., of rotational levels in the lowest vibrational states $\nu = 0, 1, 2, 3$ of a molecule (see Fig. 1) and a laser tuned in the vicinity of the vibrational frequency ω_{01} (i.e., the transition frequency between the vibrational ground state $\nu = 0$ and the first excited state $\nu = 1$). The total nonlinear susceptibility for THG is given as a sum over k resonance terms or three-photon excitation

pathways,

$$\chi^{(3)}(\omega) = \frac{n}{\epsilon_0 \hbar^3} \sum_k \frac{\mu_{10}\mu_{21}\mu_{32}\mu_{30}}{\Delta_{1P}\Delta_{2P}\Delta_{3P}}, \quad (1)$$

with the one-, two-, and three-photon detunings $\Delta_{1P} = \omega_{01} - \omega - i\gamma_{1P}$, $\Delta_{2P} = \omega_{02} - 2\omega - i\gamma_{2P}$, and $\Delta_{3P} = \omega_{03} - 3\omega - i\gamma_{3P}$, involving the laser frequency ω, the resonance frequencies ω_{ij} between two states $|i\rangle$ and $|j\rangle$, and the dephasing rates γ on the single- or multiphoton transitions. The latter define the linewidth of the corresponding resonance. The parameters μ_{ij} are the transition dipole moments for the transitions between two states $|i\rangle$ and $|j\rangle$, and n is the number density of molecules in the ground state. The latter quantity varies with temperature according to the Boltzmann distribution and, hence, permits determination of the temperature from spectra. From the third-order susceptibility, we calculate the THG power [16],

$$P_3(\omega) = \frac{3\mu_0^2\omega^2}{8\pi c_0} |\chi^{(3)}(\omega)|^2 \, |J_3(\omega)|^2 \, P_1^3 \, \exp\left[-\alpha_3(\omega)L\right], \quad (2)$$

with the fundamental laser power P_1, appearing in third order, as expected. Moreover, we find the phase-matching integral $J_3(\omega)$, which involves the effect of a wave-vector mismatch, as well as focusing conditions (for details, see Appendix). The particle density enters the equation via the nonlinear susceptibility, yielding a quadratic dependence of the THG power upon the gas pressure (provided the pressure is sufficiently low to neglect phase mismatch).

If we tune the laser to a one- two-, or three-photon resonance, one of the detunings in the nonlinear susceptibility according to Eq. (1) reduces to $|\Delta| = \gamma$ and a single term dominates in the sum for $\chi^{(3)}$. The smaller the linewidth γ, the larger the resonance enhancement $\sim 1/\gamma$ of the nonlinear susceptibility. In a gas, the linewidths are typically due to Doppler broadening and collisional broadening. In terms of spectral line shape, this corresponds to a Gaussian profile for Doppler broadening and a Lorentzian profile for collisional broadening, which results in a Voigt profile for a combination of both effects. For many gases (e.g, HCl, which we used in our experiments), Doppler broadening dominates at low absolute pressures in the mbar regime, while for higher pressures collisional self-broadening dominates. In the latter case, the line shape becomes close to Lorentzian in good approximation. At room temperature, the Doppler broadening in HCl is typically around 170 MHz (FWHM), corresponding to 0.006 cm^{-1}, expressed in units of wave numbers. This is very small compared to typical detunings of several cm^{-1} to neighbor rotational states. Therefore, we expect significant resonance enhancements in the nonlinear susceptibility. This permits selective detection of a molecular species by monitoring resonantly enhanced THG in the midinfrared molecular fingerprint regime of rovibrational transitions.

III. EXPERIMENTAL SETUP

We perform the experiments in a gas cell (length 5 cm, sealed with CaF_2 windows) at room temperature, with HCl molecules as a test gas (see Fig. 2). The gas has a purity of 99.5% with <50 ppm residual moisture (supplied by Westfalen). HCl is a relevant molecular species in combustion processes, e.g., waste combustion of polyvinyl chloride compounds [17] or biomass [18]. Due to the toxic and corrosive nature, detection of HCl even at low concentrations is highly desirable. HCl has two stable isotopes, with natural abundance of 76% in $H^{35}Cl$ and 24% in $H^{37}Cl$. The level positions and single-photon transition moments among the rovibrational levels in the electronic ground state of HCl are known from literature [19,20], which permits us to calculate nonlinear susceptibilities and numerically simulate resonantly enhanced THG in the medium. The single-photon transition wavelength between the lowest vibrational states is around 3.5 μm (corresponding to 2850 cm^{-1} expressed in wave numbers).

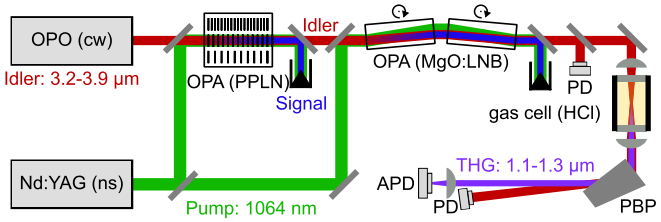

FIG. 2. Experimental setup, with optical parametric oscillator (OPO), optical parametric amplifiers (OPA), a periodically poled lithium niobate (PPLN) crystal, bulk magnesium-oxide doped lithium niobate crystals (MgO:LNB), Pellin-Broca prism (PBP), photovoltaic detectors (PD), and an InGaAs avalanche photodiode (APD).

The experiments on THG via rovibrational transition require a laser system, which combines tunable output in the midinfrared at sufficiently narrow spectral bandwidth (i.e., in the range of the Doppler broadening of 170 MHz) with large pulse energy to efficiently drive frequency conversion in the gas, also at low pressures. Toward this goal, we designed a laser system to provide tunable, midinfrared (nanosecond) laser pulses with spectral bandwidth close to the Fourier-transform limit and output pulse energy in the mJ regime.

The optical setup (see Fig. 2) involves a fiber-laser pumped, continuous wave OPO (Argos Model 2400-C, Aculight/Lockheed Martin), providing an idler wave with tunability in the spectral interval of 3.2–3.9 μm, at a spectral bandwidth of roughly 1 MHz (single longitudinal mode) and output power beyond 1 W. The OPO serves as a seed source for a homebuilt three-stage OPA system pumped by an injection seeded Nd:YAG laser (Pro Lab 230, Spectra Physics), providing laser pulses at a center wavelength of 1064 nm, pulse duration around 10 ns (FWHM) with repetition rate 20 Hz, and nearly Fourier transform-limited bandwidth.

We use a spatial filter to provide a Gaussian pump laser profile. In the first OPA stage, we apply a 5-cm-long magnesium-oxide doped periodically poled lithium niobate crystal (PPLN) (HC Photonics). The PPLN crystal contains several separated sections with different poling periods. Combined with a PID-regulated temperature control unit (HC Photonics), this permits parametric amplification in a spectral range of 3.2–4.6 μm. From the PPLN OPA stage, at a pump pulse energy of 500 μJ and 1 W seed power, we obtain nanosecond midinfrared pulses with a pulse energy around 20 μJ. We further amplify these pulses in two 3-cm-long

bulk 5% magnesium-oxide-doped lithium niobate crystals (Castech), arranged in a walk-off compensation configuration.

With a pump pulse energy of 23 mJ, we obtain a pulse energy of up to 2 mJ in the midinfrared nanosecond pulses. The beam profile of the midinfrared pulses is close to Gaussian (measured with a homebuilt moving aperture beam profiler). The idler wave is separated from the pump- and signal wave, as well as radiation from parasitic processes in the OPA chain (e.g., phase-mismatched harmonic generation of the pump- and signal wave) by dichroic mirrors and a CaF_2 Pellin-Broca prism. We note, that for continuous, single-mode tunability in a broader wavelength range, we extended the commercial cw seed OPO system with a homemade tuning unit. Precise, continuous tuning of the midinfrared wavelength is achieved by varying the central wavelength of the seed laser for the pump-laser of the OPO via temperature and piezo tuning. This enables robust operation of the system also in a broader wavelength region. As the acceptance bandwidth of the OPA crystals is rather large, fine tuning of the idler wavelength of the seed OPO in the range of 100 GHz does usually not require variation of the phase-matching conditions in the OPA stages. We apply a wavemeter (WS6, High Finesse) and a near-infrared optical spectrum analyser (OSA, AQ-6315A, Ando) to determine the pump and signal wavelength of the (signal-resonant) OPO, which in turn permits us to calculate the midinfrared idler wavelength. We verified, that the center wavelength of the obtained nanosecond pulses is equal to the wavelength of the idler wave from the seed OPO.

For further wavelength calibration of the laser system, we applied transmission measurements on single-photon resonances at a low HCl pressure (to omit pressure broadening), driven by the narrow-band cw OPO (without amplifiers) and compared the results with the HITRAN database [19]. We also determined the spectral linewidth of the amplified OPO/OPA pulses by comparison of absorption spectra obtained after cw and pulsed excitation. From such measurements, we determined a spectral linewidth of 97 MHz (FWHM, 0.003 cm^{-1} when expressed in wave numbers) for the midinfrared nanosecond pulses. This is only a factor of 2 above the Fourier-transform limit for Gaussian-shaped laser pulses with an assumed duration of 10 ns (FWHM). The deviation might be even smaller, as most probably the pulse duration of the midinfrared radiation (which we could not measure) obtained from the parametric processes is shorter than the assumed 10 ns (FWHM) of the pump pulse. Moreover, residual deviations may be due to the large gain in the first PPLN OPA stage, which adds extra bandwidth by optical parametric generation that gets subsequently amplified in the later OPA stages [21]. Nevertheless, our setup provides pulses with very small spectral bandwidth, far below typical commercial implementations for tunable, midinfrared nanosecond pulses. This is important for sufficiently large spectral resolution of molecular transitions, but even more for efficient THG due to the large spectral power density of the driving radiation.

A CaF_2 lens with a focal length of 150 mm serves to mildly focus the midinfrared laser pulses to a diameter of roughly 400 μm ($1/e^2$ of the intensity) into the HCl gas cell. We measure the absolute gas pressure in the cell with a pressure transmitter (SITRANS P200, Siemens). We monitor the pulse energy of the driving midinfrared pulses in front of the cell with an InAsSb photovoltaic detector (P13243-011MA, Hamamatsu). The integrated pulse trace of the signal was calibrated with a pyroelectric sensor (PE10-C, Ophir) to give shot-to-shot information of the fundamental pulse energy. Behind the cell, the third-harmonic wave at wavelengths of 1.1–1.2 μm is separated from the residual fundamental pulses by a CaF_2 Pellin-Broca prism, and detected on an InGaAs avalanche photodiode (IAG200S6, Laser Components), equipped with an amplifier (DLPCA-200, Femto). We use neutral density filters to reduce (if required) the THG signal fluence on the avalanche photodiode, and spectral edgepass filters (FELH1100, Thorlabs and #89-675, Edmund Optics) to suppress stray light.

IV. EXPERIMENTAL RESULTS

Figure 3 (upper row) shows an overview THG spectrum, when we tune the driving fundamental pulses in the vicinity of one-, two-, and three-photon resonances between the vibrational ground state $\nu = 0$ and excited states $\nu = 1, 2, 3$. Figure 3 (lower row) shows a transmission spectrum with one-photon resonances for comparison and frequency calibration. In the THG spectrum, we observe many strong, spectrally narrow multiphoton resonances with a large dynamic range (or signal-to-noise-ratio) of three orders of magnitude. The small background signal is mainly generated by off-resonant THG in the CaF_2 windows of the gas cell. As expected, on single-photon resonances we get only a little (if any) resonance enhancement of THG emission. In this case, the fundamental radiation is strongly absorbed—which significantly effects the THG yield due to its nonlinear dependence upon the third power of the fundamental intensity. However, we observe large THG resonance enhancements by many orders of magnitude on two-photon and three-photon resonances. Though the two-photon resonances (see spectral lines around 2830 cm^{-1}) are the strongest, we observe almost comparable resonance enhancements on three-photon resonances (see spectral lines around 2810 cm^{-1}). At first glance, the latter seems surprising, as one-photon reabsorption of the harmonic signal should reduce the THG yield on a three-photon resonance for the fundamental radiation. However, the transition moment for a one-photon overtone resonance between the vibrational ground state $\nu = 0$ and the excited state $\nu = 3$ is very small due to the small anharmonicity of the potential. We calculated the reabsorption of the THG signal to be less than 1% along the full path length in our gas cell. Thus, reabsorption of the THG signal plays no role neither for two-photon nor three-photon resonances with the fundamental field.

We analyze the resonance enhancements now in some more detail: The strongest two-photon resonance at 2830.36 cm^{-1}, labeled (A) in Fig. 3, benefits from the large thermal population of the ground state $(\nu, N_1) = (0, 3)$ (at room temperature, we have 19% of the $H^{35}Cl$-population in this state) and the larger abundance of the isotope $H^{35}Cl$. More importantly, and as already discussed in the Introduction, due to the small anharmonicity of the molecular potential, the nonlinear susceptibility is not only enhanced due to the resonant two-photon transition but also due to near-resonance conditions for the involved

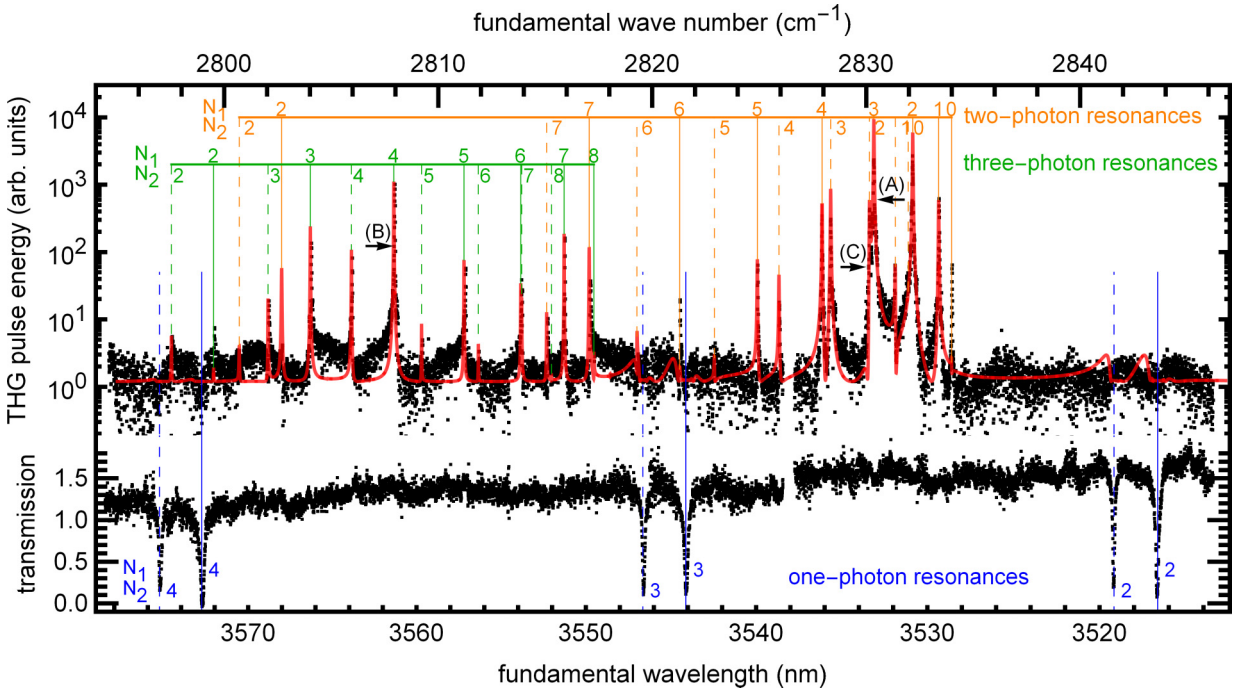

FIG. 3. Upper row: THG signal pulse energy versus fundamental laser wavelength (or wave number). HCl pressure 100 mbar, mean fundamental laser pulse energy 1.5 mJ. Black dots indicate experimental data, binned in frequency intervals of 0.005 cm^{-1}. We do not account for pulse energy fluctuations. The red line shows a numerical simulation. Vertical orange and green lines (solid line for the isotope $H^{35}Cl$, dashed for the isotope $H^{37}Cl$) indicate the frequency positions of multiphoton resonances, labeled with the corresponding rotational quantum numbers N_i of the ground rotational state in the transition (N_1: $H^{35}Cl$, N_2: $H^{37}Cl$). Note the logarithmic scale on the THG energy axis. Lower row: Transmission spectrum, driven by residual cw radiation from the OPO, with one-photon resonances indicated by blue lines. At the rather large HCl pressure used for this overview spectrum, the spectral lines are pressure broadened to roughly 1.5 GHz.

one-photon and three-photon transition. In the case of our specific two-photon resonance, the one-photon detuning from the ground state $(\nu, N_1) = (0, 3)$ to the intermediate state $(\nu, N_1) = (1, 2)$ is roughly -9 cm^{-1}, the two-photon detuning to the intermediate state $(\nu, N_1) = (2, 3)$ is zero, and the three-photon detuning to the target state $(\nu, N_1) = (3, 4)$ is -79 cm^{-1} [compare Fig. 1(a)]. Thus, also on two-photon resonance, the one- and three-photon detunings are quite small (e.g., compared to typical detunings of some 1000−10000 cm^{-1} as in CARS) and we get a large nonlinear susceptibility for THG. We note that absorption losses are still negligible, as the one-photon detunings are still large compared to the linewidth, even at larger pressure broadening (at 100 mbar we get a pressure broadening of 1.5 GHz, corresponding to 0.05 cm^{-1}).

Using transition moments from literature [19], we calculate the third-order susceptibility for the specific two-photon resonance, also including contributions from neighbor rotational states to $|\chi^{(3)}| \approx 2 \times 10^{-23}$ m^2/V^2. At a pressure of 100 mbar, the phase-matching integral yields $|J_3|^2 \approx 1.6$ (see Appendix). This is close to the maximum value of approximately 1.7, i.e., we operate close to phase-matching conditions—as expected for the weak focusing in our experiment and the small variation of the indices of refraction in the gas.

We now consider the strongest three-photon resonance at 2807.92 cm^{-1}, labeled (B) in Fig. 3. The thermal population in the ground state $(\nu, N_1) = (0, 4)$ is 16 % of the $H^{35}Cl$-population, i.e., comparable to the strongest two-photon transition, discussed above. The one-photon detuning to state $(\nu, N_1) = (1, 3)$ is roughly -9 cm^{-1} the two-photon detuning to state $(\nu, N_1) = (2, 4)$ is 40 cm^{-1} the three-photon detuning to state $(\nu, N_1) = (3, 5)$ is zero [compare Fig. 1(b)]. Thus, also in the case of the three-photon resonance enhancement, the involved single- and two-photon transitions are still quite close to resonance. This supports the nonlinear susceptibility, while absorption plays no role. We estimated the nonlinear susceptibility on the three-photon transition as $|\chi^{(3)}| \approx 7 \times 10^{-24}$ m^2/V^2. The phase-matching integral yields $|J_3|^2 \approx 1.7$, i.e., again close to perfect phase matching.

We use the calculated third-order susceptibilities (as well as first-order susceptibilities, i.e., indices of refraction and linear absorption coefficients, which are relevant for phase-matching effects) in our straightforward numerical simulations of THG to determine the THG yield versus driving laser frequency (for details, see Appendix). As the THG spectrum in Fig. 3 shows, the simulation fits well with the experimental data. However, it is no simple task to also determine from the experimental data an *absolute* value of the conversion efficiency (or THG photon numbers), as our detection setup is not calibrated. We very roughly estimated the absolute number of generated THG photons per pulse from the signal level and the estimated efficiency of the avalanche photodiode, which detects the THG wave. For the strongest two-photon resonance at $\nu = 2830.36$ cm^{-1}, under the experimental conditions of Fig. 3, we estimated a THG yield of roughly 10^7 photons per pulse. This is already a considerable amount. It fits with an order-of-magnitude estimation, taking satura-

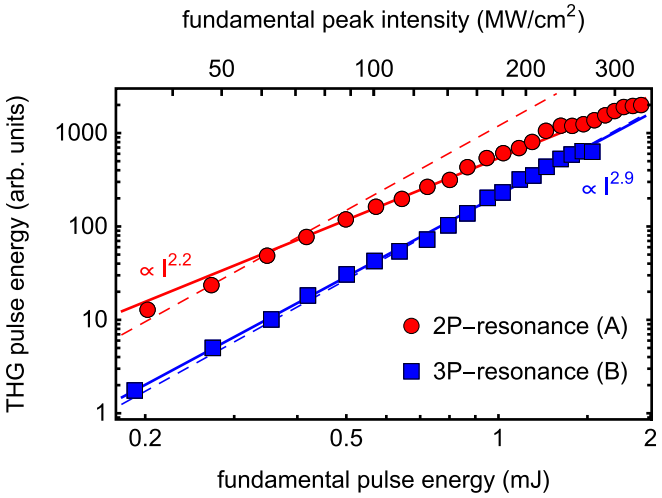

FIG. 4. THG signal pulse energy at two-photon resonance (A) or three-photon resonance (B) versus fundamental laser pulse energy (or fundamental peak intensity). Solid lines depict exponential fits to the experimental data points. For comparison, the dashed lines indicate a growth with the third power of the driving fundamental intensity. Note the double-logarithmic scale.

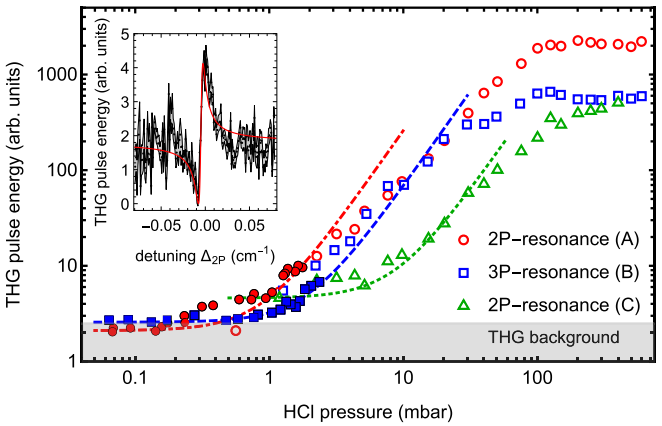

FIG. 5. THG signal pulse energy versus HCl pressure at the dominant two-photon resonance (A) or three-photon resonance (B). We also added a measurement series for larger pressures at a weaker two-photon resonance (C). The fundamental pulse energy was 1.2 mJ. Symbols indicate experimental data. The signal yield is determined as the peak value of a Lorentzian fit to the spectral line. The data consists of a measurement series mainly at larger pressures $\geqslant$ 2 mbar (indicated by hollow symbols) and measurements at lower pressures $\leqslant$2 mbar (indicated by solid symbols). Lines depict quadratic fits to the low-pressure data of all resonances. Note the double logarithmic scale. The inset shows the spectral line at the two-photon resonance (A) for a pressure of 0.6 mbar, i.e., close to the detection limit of our setup. The shaded area around the single-shot data points in the spectrum indicates the standard error. The red line indicates a fit with a Fano-type line profile.

tion of the two-photon transition into account (see below), and ignoring deviations of the driving laser beam profile from a perfect Gaussian.

To confirm the third order of the frequency conversion process, we monitored the variation of the THG pulse energy at the resonances (A) and (B) with the intensity of the driving fundamental pulses up to 350 MW/cm^2. The experimental results for the strongest two- (A) and three-photon resonance (B) are shown in Fig. 4. From an exponential fit to the data, we find an exponential coefficient of 2.9 for the signal at three-photon resonance (B), which confirms the expected cubic dependence of THG upon the driving laser intensity. However, for two-photon resonance (A) we find a significantly lower exponential coefficient of 2.2. This is due to saturation of the involved two-photon transition. From Fig. 4, we notice that our data for the two-photon resonance deviates from the expected cubic law (as indicated by the red dashed line) for intensities beyond $\approx$75 MW/cm^2. For the latter intensity, we calculate a two-photon Rabi-frequency $\Omega_{2P} \approx 2\pi \times 102$ MHz. This intensity corresponds to a pulse area of $\Omega_{2P} \times \tau \approx 6.4$, with the laser pulse duration τ. The condition $\Omega_{2P} \times \tau \gg 1$ indicates the onset of saturation and, hence, confirms the observed deviation of the intensity dependence for the THG yield at two-photon resonance.

Finally, we note that our simulation (see red line in Fig. 3) confirmed all major spectral lines in the experimental data with only two smaller exceptions: The simulation also predicted a two-photon resonance of moderate line strength at 2802.7 cm^{-1} (H^{35}Cl, $N_1 = 2$)—though we did not observe it. On the other hand, we observed a two-photon resonance at 2834.0 cm^{-1} (contribution from H^{35}Cl with $N_1 = 0$), which proved to be stronger then expected by the simulation. Apart from these findings, the vast majority of the data is very well described by the simulation in Fig. 3.

To determine the detection limit of the THG approach in our setup with regard to the HCl pressure, we performed systematic measurements of the THG yield versus pressure at two- and three-photon resonances (see Fig. 5). Under conditions of perfect phase matching, we would expect the signal intensity to grow quadratically with the number density or pressure. This is confirmed by the pressure dependence at the two-photon resonances (A,C) as well as at the three-photon resonance (B) in Fig. 5 for pressures below a few 10 mbar. Only the two-photon resonance (A) shows some deviation from the quadratic dependence in the pressure range above 10 mbar (see dashed, dotted red line in the plot). For an exponential fit to the data below the plateau region at resonance (A), we get an exponent of $\approx$1.44 rather than 2. Nevertheless, in the regime of smaller pressures $\leqslant$ few mbar, the data at resonance (A) also follow the quadratic dependence in good approximation.

For larger pressures above 50−100 mbar, the THG yield does not grow anymore with increasing pressure, but remains on an (almost) constant level for all multiphoton resonances (A,B,C). This is due to pressure broadening. The numerator of $\chi^{(3)}$ in Eq. (1) has a linear dependence upon the number density n (or pressure). In the case of resonant THG, Eq. (1) is dominated by the decay rate. At sufficiently large pressure, the decay rate is given by collisional broadening and also increases linearly with pressure. Therefore, the pressure dependence in $\chi^{(3)}$ cancels when collisional broadening dominates. Due to the weak focusing conditions in our experimental setup, phase matching does not significantly influence

the dependence of the THG energy on the pressure (compare Appendix).

As the data in Fig. 5 shows, at the strong two-photon resonance (A), we still get a signal-to-background ratio of approximately 1 for a pressure of 0.6 mbar (see inset in the figure). We get clearly detectable THG signals above the THG background down to pressures of 0.1 mbar. In this case, we already operate at the detection limit of the APD. Hence, we can define a conservative detection limit for the THG approach in our setup in the range $\leqslant$1 mbar, where the THG energy is well separable from the THG background. This pressure corresponds to roughly 3×10^{13} molecules in the interaction volume of the fundamental radiation, corresponding to a particle density of 10^{15} molecules/cm^3. We took into account that the THG signal was obtained from a fraction of the HCl molecules in the interaction volume, i.e., the isotope $H^{35}Cl$ in the rotational ground state $N_1 = 3$.

A fair comparison of the obtained detection limit to other nonlinear spectroscopy techniques is no simple task, as not only the nonlinear susceptibility but also the specific conditions of the laser and detection setup are relevant. Typically, detection limits of 0.1 to 1 mbar are obtained for CARS detection of diatomic molecules in combustion when suppressing the nonresonant CARS background [1,22]. In an experiment on detection of HCl molecules by degenerate four-wave mixing driven by midinfrared (ns) laser pulses with pulse energies up to 2 mJ, and similar intensity in the interaction region as in our setup, Sun *et al.* achieved a detection limit of 6.8×10^{14} molecules/cm^3 [23]. Hence, the detection limit, which we obtained for resonantly enhanced THG, will already permit realistic applications for trace gas analytics. We must not fail to mention that our measurements were performed in a gas cell with pure HCl, i.e., without any background gas—which would be present under typical conditions of trace gas analytics. Collisional broadening induced by the background gas would increase the decay rate in Eq. (1) and reduce the obtained THG resonance enhancement. Moreover, phase matching in the background gas will vary (increase or decrease) the THG yield. However, there are still means to further improve the detection limit to compensate for the effects of background gas: In our setup, we were limited by the nonresonant THG background from the CaF_2 windows (which we confirmed to also remain in an evacuated gas cell). The latter are not required in setups with gas flows or flames. This would enable us to approach a detection limit determined only by the quantum efficiency of the detector. Moreover, more available laser pulse energy, larger laser bandwidth (matched to the larger, collision-broadened spectral linewidth), and optimized focusing conditions matched to the low-pressure regime would further improve the detection limit.

We now consider the spectral line profiles on resonances (A) and (B) at lower HCl pressures close to the detection limit in more detail (see Fig. 6, data taken at a pressure of 1 mbar). Obviously, the spectral line shapes are asymmetric and quite different from a Gaussian profile expected for a nearly only Doppler-broadened spectral line. Such asymmetric, Fano-type resonances are known from other types of nonlinear spectroscopy [24]. They are due to interference, in our case between the resonant THG signal from HCl and

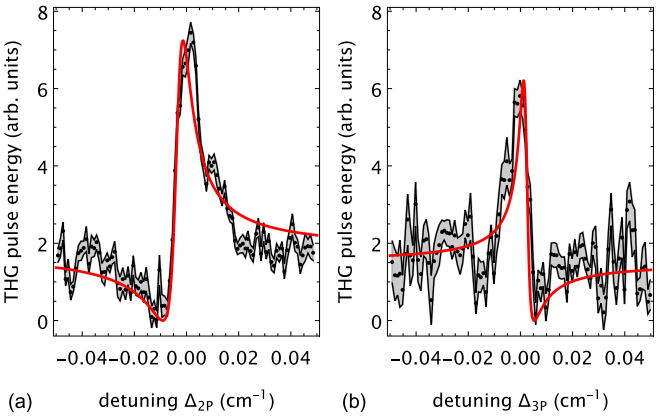

FIG. 6. THG signal pulse energy versus fundamental laser detuning at low HCl pressure of 1 mbar and fundamental laser pulse energy around 1 mJ. Spectral lineshapes of (a) two-photon resonance (A) and (b) three-photon resonance (B). The signal offset is due to off-resonant THG background. Black dots indicate experimental data, red solid lines show Fano fits, shaded areas depict the standard error for binning in frequency intervals of 0.001 cm^{-1}.

the THG background from the CaF_2 windows. Hence, we cannot simply subtract the measured background from the empty cell to further reduce the detection limit. To the data points in Fig. 6 we fit Fano-type profiles according to $f(\epsilon) \sim (\epsilon + q)^2/(\epsilon^2 + 1)$ with the detuning $\epsilon = 2\Delta/\Gamma$, a linewidth factor Γ, and the Fano-parameter q. The fit to resonance (A) yields $q = 1.7$, while for resonance (B) we get $q = -1.8$ (see Fig. 6). In a very rough estimation for a Fano profile, the value $|q|^2$ is determined by the ratio of resonant and background signal. Hence, the fit values for the Fano parameters mirror the observed signal-to-background ratios of approximately 3−4 for the two spectral lines (A, B) at low pressure, not far from the detection limit of our setup. We note that in the limit $q \to \infty$, a Fano profile is well approximated by a symmetric Lorentzian (yielding a near-Gaussian profile when we take Doppler broadening into account). Therefore, we found that the asymmetric Fano profile is only observable for quite low pressures. It evolves into a symmetric line shape for HCl pressures beyond 5 mbar, when the resonant THG signal becomes much larger compared to the THG background.

As collisional broadening increases the spectral linewidth and, hence, reduces the spectral resolution and detection limit, we performed extended measurements on the variation of the spectral linewidth with the HCl pressure. Figure 7 shows the variation of the THG pulse energy with both driving laser wave number and pressure compared to a numerical simulation. The data already shown in Fig. 5 are a fraction of this larger, two-dimensional data set. The two resonances, (C) and (A) corresponding to $H^{37}Cl$ and $H^{35}Cl$, are clearly distinguishable in the data. Below 20 mbar, pressure-induced broadening of the lines is negligible compared to the Doppler linewidth. Note the asymmetric line shape at low pressures, as already discussed above. With increasing pressure, the linewidth (FWHM) of both spectral lines increases linearly due to collisional broadening, as expected and confirmed by the simulation. For HCl pressures between 50 mbar up to 650 mbar, we measure a self-broadening coefficient for reso-

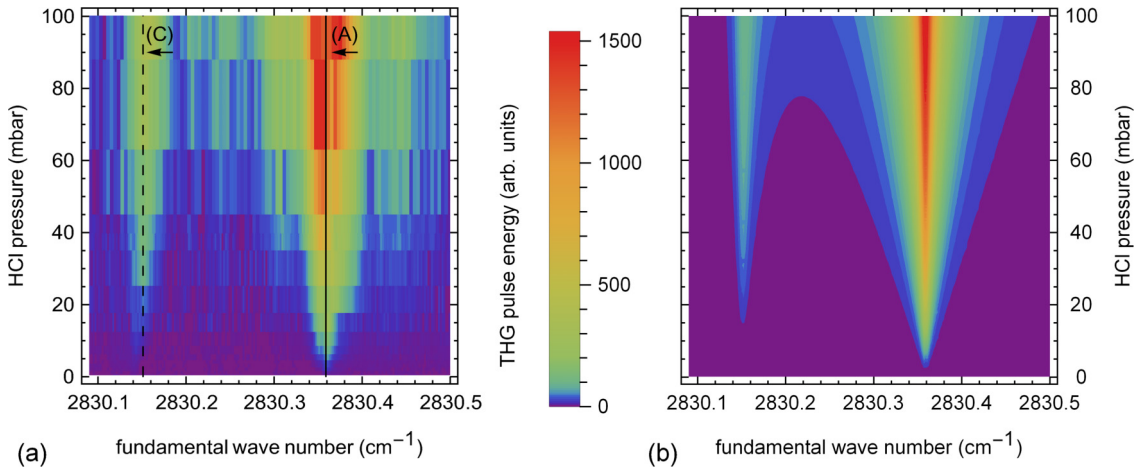

FIG. 7. (a) Experimental data: THG signal pulse energy versus HCl pressure and fundamental laser wave number in the vicinity of the two-photon resonances (C) and (A). We show a fraction of the available experimental data, i.e., for pressures below 100 mbar. Black vertical lines indicate the expected spectral positions of the two-photon resonances (solid line for $H^{35}Cl$, dashed line for $H^{37}Cl$). (b) Numerical simulation. For better comparison, the absolute intensity is normalized to the peak intensity in the experimental data.

nance (A) of 0.230 cm^{-1}/bar. This is in good agreement with the simulation value of 0.227 cm^{-1}/bar and with literature values based on two-photon absorption, which give a coefficient of 0.225(3) cm^{-1}/bar [25].

The simulation includes line broadening but omits possible pressure-induced shifts of the resonance position as the required collision parameters for the linear pressure shift are not completely available. From literature values based on two-photon absorption measurements, we roughly expect a shift coefficient in the range of $\pm 0.02\,cm^{-1}$/bar (which also depends upon the rotational state) [25] for the $H^{35}Cl$ isotope. Hence, the pressure-induced shift should be quite small in our pressure range. This is confirmed by the experimental data: For resonance (A), we observe a small pressure shift of $-0.018\,cm^{-1}$/bar for HCl pressures beyond 60 mbar. For resonance (C) in the isotope $H^{37}Cl$, we observe a small shift by $-0.040\,cm^{-1}$/bar in this pressure range. Beyond these findings, the data confirms the high resolution of THG spectrometry in our setup, which permits us to well resolve and quantify the two HCl isotopes (as a test example for two molecular species) also at larger pressures.

In summary of the discussion above, the detection limit which we obtained in THG mid-IR spectroscopy with narrowband (ns) pulses clearly indicates the potential of the approach for realistic applications in trace gas analysis. In particular, this will hold true for molecules with much larger nonlinear susceptibilities compared to our test gas HCl. As an example, for THG in the vibrational asymmetric stretch mode ν_3 of CO_2, we get a nonlinear susceptibility at two-photon resonance at a fundamental wavelength of 4.3 μm in the order of 10^{-21} m^2/V^2, two orders of magnitude larger than in HCl.

V. CONCLUSION AND OUTLOOK

We presented extended experimental studies on resonantly enhanced THG driven by midinfrared, spectrally narrowband, nanosecond laser pulses tuned in the vicinity of rovibrational molecular resonances with HCl molecules as a test gas. In contrast to other approaches for nonlinear spectroscopy, the technique requires only a single driving laser beam, which facilitates applications. The driving radiation is provided by a laser system, based upon pulsed, multistage optical parametric amplification of the idler output of a single-mode OPO. The laser setup delivers nanosecond midinfrared pulses with pulse energies up to 2 mJ, small spectral bandwidth $\leqslant$100 MHz (FWHM), i.e., only a factor of 2 above the Fourier transform-limit, and broad continuous tunability in the midinfrared. For the experiments, we operate under mild focusing conditions, yielding laser intensities up to 350 MW/cm^2. As a major advantage of the THG approach among rovibrational states in the electronic ground state of the molecules, we drive the frequency conversion process simultaneously close to single-, two-, and three-photon resonances, with typical detunings in the range of 10–100 cm^{-1} only. Tuning exactly to a single-photon resonance is, due to absorption of the fundamental radiation, no good choice. Tuning to two- and three-photon resonances permits large resonance enhancements of the THG yield by up to three orders of magnitude with regard to the background signal. We compare the experimental results to a straightforward numerical simulation, which agrees well with the data. We systematically study and compare THG via two- and three-photon resonances in HCl. We find that saturation of the two-photon transition and resonance enhancements occur for laser intensities beyond 75 MW/cm^2, while we do not yet observe such saturation at our available laser intensities for the higher-order, three-photon transition. Measurements of the THG signal with sample pressure confirm the quadratic dependence expected for a nonlinear optical process. At large pressures beyond a few 10 mbar, collisional broadening leads to saturation of the signal versus sample pressure. A detailed analysis of the spectral line shape shows an asymmetric, Fano-type line profile at lower gas pressures, which is due to interference between the resonant signal from the test gas and nonresonant background. The asymmetry vanishes at higher pressures due to collisional broadening, giving rise to a symmetric line profile. From the pressure dependence, we determine a detection limit for the THG approach in the HCl sample in the range of $\leqslant$1 mbar,

corresponding to roughly 3×10^{13} molecules in the confocal volume of the driving laser field, or a particle density of 10^{15} molecules/cm^3. This permits applications of the approach under realistic conditions of trace gas detection.

ACKNOWLEDGMENTS

We acknowledge experimental assistance by J. S. Otto, F. Pelz, and O. Ernst, support with the numerical simulations by N. Stewen, valuable discussions with C. Stock, as well as financial support by the Deutsche Forschungsgemeinschaft (DFG).

APPENDIX: NUMERICAL SIMULATION

We calculate the THG yield on the multiphoton resonances in HCl using Eq. (2). The latter involves the nonlinear susceptibility $\chi^{(3)}(\omega)$, the phase matching integral J_3, the fundamental laser power P_1, and the absorption coefficient α_3 for the generated third harmonic.

The nonlinear susceptibility $\chi^{(3)}(\omega)$ is given by Eq. (1). The sum includes all allowed optical dipole transitions in the electronic ground state of both HCl isotopes (with selection rules $\Delta N_i = \pm 1$, $\Delta\nu = \pm 1$) and all possible permutations in the four-wave mixing scheme [15]. We constrained the calculation to a maximum vibrational quantum number of $\nu = 3$. The population in the vibrational ground state $\nu = 0$ is thermally distributed over the rotational states according to the normalized Boltzmann distribution $(2N_i + 1)/Z \exp[-E_{\mathrm{rot}}/(k_{\mathrm{B}}T)]$, with the Boltzmann constant k_{B}, the energies of the rotational ground states E_{rot}, and the sum over all populations Z as the normalization factor. We considered rotational ground states up to a relative population down to 10^{-5}, which corresponds to a maximum rotational quantum number of $N_1 = 14$ at room temperature (25 °C) for the isotope $H^{35}Cl$. This fully covers the observed rotational transitions in our spectra (compare Fig. 3). The number density in Eq. (1) is calculated from the ideal gas equation. Temperature, HCl pressure, isotopic abundance, and relative population of the rotational ground state were taken into account.

The phase-matching integral J_3 for the case of THG [26–28] is given by

$$J_3 = \frac{2}{b}\int_0^L \frac{\exp[-i\Delta k z]}{(1 + 2i(z - z_0)/b)^2} dz, \tag{A1}$$

where $b = 2\pi w_0^2/\lambda$ is the confocal parameter of the fundamental radiation (in our setup $b = 6$ cm), L the length of the gas cell, and z_0 the position of the focus. The wave-vector mismatch is given by $\Delta k = k_3 - 3k_1$, with $k(\lambda, p, t) = 2\pi/\lambda\sqrt{1 + \chi^{(1)}(\lambda, p, t)}$. Note that the wave vectors are assumed as complex quantities. The imaginary part of $\sqrt{1 + \chi^{(1)}(\lambda, p, t)}$ is proportional to the linear absorption coefficient $\alpha(\lambda, p, t) = 2\mathrm{Im}[k(\lambda, p, t)]$. Absorption, in particular, of the fundamental wave, substantially reduces the value of the phase matching integral in the vicinity of one-photon resonances. In our simulations, we calculated the linear susceptibility from HITRAN data. We note that the estimations of the phase-matching integral at resonances (A,B), as discussed above (see Sec. IV) also involved an offset in the real part of the linear susceptibility, which is due to a nonresonant contribution via the far-detuned electronic transitions in the UV range [29,30]. For simplicity, we assumed this offset to be independent of pressure and temperature.

To obtain spectral line profiles, we assume a Lorentzian shape of a width determined by the dephasing rates $\gamma_{1\mathrm{P}}$, $\gamma_{2\mathrm{P}}$, and $\gamma_{3\mathrm{P}}$ [see Eq. (1)]. The latter are determined by Doppler-broadening, collisional broadening, and laser linewidth.

[1] S. A. Druet and J. P. E. Taran, Prog. Quantum Electron. **7**, 1 (1981).
[2] J. Wolfrum, Symp. Combust. **27**, 1 (1998).
[3] M. Müller and A. Zumbusch, ChemPhysChem **8**, 2156 (2007).
[4] P. D. Maker and R. W. Terhune, Phys. Rev. **137**, A801 (1965).
[5] R. Carriles, D. N. Schafer, K. E. Sheetz, J. J. Field, R. Cisek, V. Barzda, A. W. Sylvester, and J. A. Squier, Rev. Sci. Instrum. **80**, 081101 (2009).
[6] D. M. Bloom, J. T. Yardley, J. F. Young, and S. E. Harris, Appl. Phys. Lett. **24**, 427 (1974).
[7] R. Hilbig and R. Wallenstein, IEEE J. Quantum Electron. **17**, 1566 (1981).
[8] R. A. Ganeev, M. Suzuki, M. Baba, H. Kuroda, and I. A. Kulagin, Appl. Opt. **45**, 748 (2006).
[9] V. Petrov, Prog. Quantum Electron. **42**, 1 (2015).
[10] Y. Miyamoto, H. Hara, T. Hiraki, T. Masuda, N. Sasao, S. Uetake, A. Yoshimi, K. Yoshimura, and M. Yoshimura, J. Phys. B At. Mol. Opt. Phys. **51**, 015401 (2018).
[11] A. A. Makarov and E. A. Ryabov, Uspekhi Fiz. Nauk **189**, 271 (2019).
[12] A. J. Traverso, B. Hokr, Z. Yi, L. Yuan, S. Yamaguchi, M. O. Scully, and V. V. Yakovlev, Phys. Rev. Lett. **120**, 063602 (2018).
[13] J. A. Armstrong, N. Bloembergen, J. Ducuing, and P. S. Pershan, Phys. Rev. **127**, 1918 (1962).
[14] R. W. Boyd, *Nonlinear Optics*, 3rd ed. (Academic Press, New York, 2008), p. 640.
[15] G. S. He, *Nonlinear Optics and Photonics* (Oxford University Press, Oxford, 2014).
[16] H. Kildal and T. F. Deutsch, IEEE J. Quantum Electron. **12**, 429 (1976).
[17] A. A. Stec, T. R. Hull, K. Lebek, J. A. Purser, and D. A. Purser, Fire Mater. **32**, 49 (2008).
[18] X. Ren, R. Sun, H. H. Chi, X. Meng, Y. Li, and Y. A. Levendis, Fuel **200**, 37 (2017).
[19] I. E. Gordon, L. S. Rothman, C. Hill, R. V. Kochanov, Y. Tan, P. F. Bernath, M. Birk, V. Boudon, A. Campargue, K. V. Chance, B. J. Drouin, J. M. Flaud, R. R. Gamache, J. T. Hodges, D. Jacquemart and others, J. Quant. Spectrosc. Radiat. Transf. **203**, 3 (2017).
[20] G. Li, I. E. Gordon, P. F. Bernath, and L. S. Rothman, J. Quant. Spectrosc. Radiat. Transf. **112**, 1543 (2011).
[21] Y. Miyamoto, H. Hara, T. Masuda, T. Hiraki, N. Sasao, and S. Uetake, Jpn. J. Appl. Phys. **56**, 032101 (2017).
[22] A. C. Eckbreth, *Laser Diagnostics for Combustion Temperature and Species* (Gordon and Breach, London, 1996)

[23] Z. W. Sun, Z. S. Li, B. Li, M. Aldén, and P. Ewart, Appl. Phys. B Lasers Opt. **98**, 593 (2010).
[24] K. M. Murdoch, D. E. Thompson, K. A. Meyer, and J. C. Wright, Appl. Spectrosc. **54**, 1495 (2000).
[25] G. Li, A. Serdyukov, M. Gisi, O. Werhahn, and V. Ebert, J. Quant. Spectrosc. Radiat. Transf. **165**, 76 (2015).
[26] J. F. Ward and G. H. C. New, Phys. Rev. **185**, 57 (1969).
[27] G. C. Bjorklund, IEEE J. Quantum Electron. **11**, 287 (1975).
[28] A. Lago, G. Hilber, and R. Wallenstein, Phys. Rev. A **36**, 3827 (1987).
[29] R. Rollefson and A. H. Rollefson, Phys. Rev. **48**, 779 (1935).
[30] J. E. Chamberlain, F. D. Findlay, and H. A. Gebbie, Appl. Opt. **4**, 1382 (1965).